CHIN. PHYS. LETT. Vol. 36, No. 11 (2019) 114302

Acoustic Vortex Beam Generation by a Piezoelectric Transducer Using Spiral Electrodes *

Han Zhang(张晗)[1**], Yang Gao(高阳)[2]

[1]Key Laboratory of Noise and Vibration, Institute of Acoustics, Chinese Academy of Sciences, Beijing 100190
[2]College of Science, China Agricultural University, Beijing 100083

(Received 19 June 2019)

We propose an innovative method to generate acoustic vortex waves based on a disc piezoelectric transducer that is coated with multi-arm coiled electrodes. Finite element simulation results for single-arm to four-arm coiled electrodes indicate that the method could modulate amplitude and phase spatial distribution of the acoustic waves near the acoustic axis by acoustic field synthesis principle, making the waves rotate spirally in space and form stable focused vortex beams. Compared with the traditional method that requires electronic control of an array consisting of a large number of transducers, this method provides a more effective and compact solution.

PACS: 43.20.+g, 47.32.−y, 43.38.−p, 02.70.Dh DOI: 10.1088/0256-307X/36/11/114302

Acoustic waves with screw wavefront dislocation are known as acoustic vortex beams, which are able to carry orbital angular momentum (OAM). In the wavefront dislocation of a screw monochromatic continuous traveling acoustic wave beam, there is a spiral phase $\exp(i\ell\theta)$ that is linearly proportional to the azimuthal angle θ, where the integer ℓ is called 'topological charge' or the order of the screw beam. The sign and the value of ℓ determine the orientation of the spiral and the magnitude of the OAM, respectively.[1−3]

In recent years, acoustic vortex beams have attracted considerable attention, showing great potential for applications of particles trapping, acoustic levitation, contact-less manipulation and high-speed acoustic communication.[4−13] Acoustic vortex beams have unprecedented combination of selectivity and trapping force. Non-contact transfer of the angular momentum enables them to be used as acoustic wrenches.[11] The circular distribution of acoustic power enables them to trap particles as acoustic tweezers.[5,12,13] The topological charges of OAM provide intrinsically orthogonal channels, which indicates a great potential of channel multiplexing in acoustic communication.[4,10]

There are two basic methods to produce desired acoustic field. The first is designing specific transducers or transducer arrays to transmit the required acoustic beams,[14−16] such as annual focus transducers.[14] The second is designing specific passive structures to modulate the amplitude, phase or path of the acoustic wave propagating in them,[17,18] such as acoustic grating.[18] Therefore, acoustic vortex beams are usually generated by active methods with phase-array transducers electrically or passive structures physically.[1] The phase-spiral source consists of an array of individually addressed transducers which are excited with appropriate screw phases to produce the expected phase profile in acoustic vortex beams.[4,19,20] Its disadvantage is the need of sophisticated electronic control, which causes substantial difficulty in integration and is expensive.[21] The physical spiral source produces acoustic vortex beams using a passive structure with screw dislocated profiles.[1,3,22−25] It avoids sophisticated electronic control, but it needs elaborate spiral profiles and may also have a bulky size. For example, Jiang *et al.*[25] used a disc with multi-arm coiling slits, which is a passive structure similar to optical grating. A transmitting transducer produced plane waves, and then the disc fixed in front of the transducer was used to modulate the amplitude and phase of the waves in the diffraction field to transform them into vortex beams. In addition to these methods, Jiang *et al.*[1] also used acoustic resonances in a planar layer with simple structure to twist wave vectors of an in-coming plane wave into a spiral phase dislocation of an outgoing vortex beam, while it still needs to select alternative materials and carry out further experiments for underwater propagation. Therefore, a more effective and generally applicable method with more compact transducer system is needed.

In this Letter, an innovative method is proposed to satisfy the demand, based on piezoelectric transducer coated with multi-arm coiled spiral electrodes, which is more compact than other phase-spiral sources[4,19,20] and easier to prepare than other passive structures.[1,3,22−25] In this method, the phases of the acoustic beams are controlled by the design of the electrodes, and then a focused acoustic vortex is generated with beam synthesis principle. That is to say, the piezoelectric transducer can produce vortex beams directly, indicating higher accuracy compared with the passive methods,[1,3,22−25] where the acoustic vortex beams are formed by the delay phase difference of acoustic waves propagating in the structure. Moreover, the two separate components,[25] the transmitting transducer and the disc with multi-arm coiling slits, are synthesized together into a piezoelectric disc

*Supported by the National Natural Science Foundation of China under Grant Nos 11772349, 11472299, 51704015, 11972354 and 11972365 and the China Agricultural University Education Foundation under Grant No 1101-240001.
**Corresponding author. Email: zhanghan@mail.ioa.ac.cn
© 2019 Chinese Physical Society and IOP Publishing Ltd

in this work, indicating that our acoustic source is more compact and easier to install. Using the finite element simulation software, the acoustic field excitation characteristics of the piezoelectric transducer are studied and analyzed. The results show that our proposed method is able to generate an acoustic vortex with the advantages of simple operation, general applicability, great compactness with low cost. This study provides theoretical basis for promoting the practical application of acoustic vortex beams in manipulation of particles, micro-organisms, cells and acoustic communication in the future.

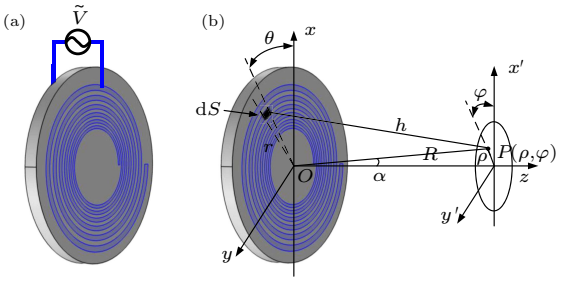

Fig. 1. (a) Schematic diagram of transducer based on multi-arm coiled spiral electrodes, and (b) working principle of radiating acoustic vortex field.

Figure 1 shows a schematic diagram of the transducer coated with multi-arm coiled spiral electrodes and its working principle of radiating acoustic vortices field. Different points of the electrodes on transducer disc radiate the same frequency acoustic wave. The amplitude and phase spatial distribution of the wavefront are affected by the difference of wave path, thus a stable focused acoustic vortex can be synthesized in the small radiation space around the acoustic axis.

For a piezoelectric disc, one of the surfaces is coated with the electrode for total area and connected to ground in the actual drive. We coat the other surface with the multi-arm spiral electrodes and apply sinusoidal voltage with the same frequency and phase to drive the piezoelectric disc. Its operation is much simpler than the using transducer arrays to generate vortex. Logarithmic Helix, $r = ae^{b\theta}$ in polar coordinates, is chosen as the helix function of the spiral arm electrodes, where r is the radial coordinate, θ is angle coordinate, a is initial radius, and b is the azimuth coefficient, which indicates the growth rate of radial distance with the increase of angle. The helix expressions of the inner and outer edges lines of the electrode bars are

$$r_1 = a_1 e^{b\theta},\ r_2 = a_2 e^{b\theta},\ \theta \in [\theta_1, \theta_2], \tag{1}$$

which have different initial radii a_1 and a_2, and θ_1 and θ_2 are termination angle and origin angle, respectively. Without loss of generality and for the sake of simplicity, we first introduce the structure and sound field of transducer coated with single-arm electrode which is capable of generating vortex beams with a topological charge $\ell = 1$. The origin is the central point of the circular area on the disc surface. The initial radii a of inner and outer edges are 13.8 mm and 14.85 mm, respectively. The azimuth coefficient b is designed to be 0.0225. The angle θ rotates from 0 to 12π. In the structure shown in Fig. 1, the piezoelectric material is PZT-4 and the transducer is 1 mm thick. The material of coated electrode is set to silver. The width of the electrode bar d decides the available frequency bandwidth of the transducer. This can produce acoustic vortex beams with the wavelength in the range of $[2d_{\min},\ 2d_{\max}]$. For the one-armed coiling electrode bar, $d_{\min} = 1$ mm and $d_{\max} = 2.47$ mm, which determine that the corresponding low and high critical frequencies are 305 kHz and 750 kHz. The operating frequency is 425 kHz in this study. According to the relationship between electrode widths and critical frequencies,

$$d_{\max} = \frac{c}{2f_{\min}},\quad d_{\min} = \frac{c}{2f_{\max}}, \tag{2}$$

a wider frequency bandwidth $[f_{\min}, f_{\max}]$ is obtained by enlarging $d_{\max}$ or reducing $d_{\min}$. In this work, when the excitation voltage is applied to drive the spiral electrodes, the coated area generates longitudinal vibration through piezoelectric effect, and then the sound waves is radiated into space and the focused acoustic vortex beam is synthesized near the acoustic axis.

In the theoretical model shown in Fig. 1(b), the spiral electrode can be regarded as an isopotential line. Therefore, the amplitude and phase of the vibration generated by the electric excitation are the same at every point on the surface of spiral electrode. It is assumed that the piezoelectric disc is embedded in an infinite baffle plate. The coordinate origin O is set at the center of the acoustic radiation surface of the piezoelectric disc, and the polar coordinates of the plane is represented by r and θ, while the observation plane at the distance z is represented by ρ and φ. A certain observation point P is set in the observation plane. The angle between the position vector of P and the z axis is represented by α. The Rayleigh–Sommerfeld diffraction integral is used to calculate the acoustic pressure at the observation point P. The normalized pressure at P is calculated by

$$p(\rho,\varphi,z) = v_a \rho_0 c_0 \int_{\theta_1}^{\theta_2} \int_{a_1 e^{b\theta}}^{a_2 e^{b\theta}} \frac{i\omega\rho_0}{2\pi h} e^{i(\omega t - kh)} r dr d\theta, \tag{3}$$

where ρ_0 is the density of acoustic transmission medium, c is sound velocity in the medium, ω is the angular frequency of vibration of the particle on the surface of the transducer, $k = 2\pi/\lambda$ is the wave number, and $\lambda = c/f$ is the wavelength of acoustic wave in acoustic transmission medium. There is no limitation on acoustic transmission medium, that is to say, this transducer system is generally applicable. Here, h is the distance between the observation point P and the surface element $dS = rdrd\theta$ in the spiral electrode,

$$h = \sqrt{\rho^2 + r^2 + z^2 - 2rR\cos\varphi\sin\alpha}, \tag{4}$$

where R is the straight-line distance between the observation point P and the origin point O,

$$R = \sqrt{\rho^2 + z^2}. \tag{5}$$

Similarly, transducers coated with multi-arm coiled spiral electrodes are obtained. The expression of inner and outer edge lines of spiral electrodes is $r = ae^{b\theta}$, which is the same as the single-arm electrode. The parameters of the spiral electrodes coated on four transducers are listed in Table 1, which can produce acoustic vortices with topological charges of 1, 2, 3 and 4, respectively. According to the largest and smallest widths of the electrode bars, the low and high critical frequencies are 305 kHz and 750 kHz for the four cases.

Table 1. Parameters of the spiral electrodes.

Number of spiral arms	Initial radius of inner edge a_1	Initial radius of outer edge a_2	Azimuth coefficient b	Origin angle θ_1	Termination angle θ_2
1	13.8 mm	14.85 mm	0.0225	0	12π
2	13.8 mm	14.85 mm	0.0451	0	6π
3	13.8 mm	14.85 mm	0.0676	0	4π
4	13.8 mm	14.85 mm	0.0902	0	3π

The synthetic acoustic field excited in space with $\ell = 1$ can be calculated by Eq. (3), which can be extended to the case of two-arm electrodes. The helix expression of inner and outer edges for one of the electrodes is $r = ae^{b\theta}$. The origin angle difference between the helices of two electrodes is π. Thus the helix expression for the other electrode is $r = ae^{b(\theta+\pi)}$. The acoustic field caused by each electrode is similar to the case of single-arm electrode. According to Eq. (3), the synthesis acoustic field is obtained as

$$\begin{aligned} &p_{\ell=2}(\rho,\varphi,z) \\ &= v_a\rho_0 c_0 \int_{\theta_1}^{\theta_2}\int_{a_1e^{b\theta}}^{a_2e^{b\theta}} \frac{i\omega\rho_0}{2\pi h} e^{i(\omega t-kh)} r dr d\theta \\ &\quad + \int_{\theta_1}^{\theta_2}\int_{a_1e^{b(\theta+\pi)}}^{a_2e^{b(\theta+\pi)}} \frac{i\omega\rho_0}{2\pi h} e^{i(\omega t-kh)} r dr d\theta. \end{aligned} \tag{6}$$

Then Eq. (6) is extended to the case of circular piezoelectric transducer coated with multiple-arm coiled spiral electrodes as follows:

$$\begin{aligned} &p_\ell(\rho,\varphi,z) \\ &= v_a\rho_0 c_0 \sum_{n=1}^{\ell}\int_{\theta_1}^{\theta_2}\int_{a_1e^{b[\theta+\frac{2\pi(n-1)}{\ell}]}}^{a_2e^{b[\theta+\frac{2\pi(n-1)}{\ell}]}} \frac{i\omega\rho_0}{2\pi h} e^{i(\omega t-kh)} r dr d\theta. \end{aligned} \tag{7}$$

To verify this method, we use finite element simulation to obtain the solution of Eq. (7) and analyze the amplitude and phase distribution of the acoustic pressure field on the observation plane. The finite element method (FEM) has been widely used in acoustic field calculation to solve multiphysics coupling problems.[26–28] In this work, the acoustic radiation of a piezoelectric ceramic disc with 1–4 coiled arm electrodes in water is simulated in the coupling multi-physics fields. The sound velocity in water is 1500 m/s, and its density is 1000 kg/m^3. In the physical field of solid mechanics, the piezoelectric material is PZT-4. The diameter and the thickness of the ceramic disc are 38 mm and 1 mm, respectively, indicating the compactness of this system without the necessity of extra integration cost. In the electrostatic field, the surface of the piezoelectric circular plate with spiral electrodes is set near the water and its electric potential is set 100 V. The surface with fully coated electrode is further from the water and set grounded. The excited acoustic pressure field at frequency 425 kHz is simulated and observed in the frequency domain. The outer surface of the water area radiates spherical wave corresponding to the thickness vibration mode of the piezoelectric ceramic disc. The models of piezoelectric ceramic discs with four kinds of electrode-coating structures are shown in Fig. 2. The blue areas are the coated spiral electrodes. In the simulation, the spiral strip electrode is modeled as isopotential.

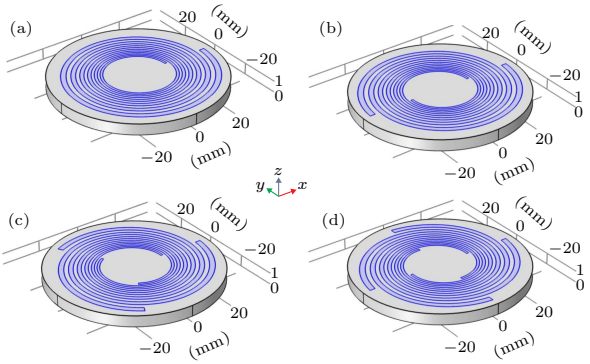

Fig. 2. Simulation models of transducers coated with (a) single-arm, (b) two-arm, (c) three-arm, and (d) four-arm coiled spiral electrodes.

With the increase of the numbers of spiral electrodes, we can obtain acoustic vortex beams with larger topological charge l, while there is a limitation of the largest topological charger $\ell_{\max}$, which is mainly decided by the radius of piezoelectric disk, and meanwhile related to frequency bandwidth.

The following derivation uses Eq. (1). The smallest and largest widths of the electrode bars, $d_{\min}$ and $d_{\max}$, which are decided by the frequency bandwidth according to Eq. (2), are

$$d_{\min} = a_2 - a_1, \quad d_{\max} = (a_2 - a_1)e^{b\theta_2} = d_{\min}e^{b\theta_2}. \tag{8}$$

The spiral electrodes and the piezoelectric disk satisfy the following geometrical constraint conditions, from which the largest topological charge $\ell_{\max}$ is deduced. Firstly, the radius of piezoelectric disk R should be greater than the largest radius of outer edge of the electrode bar $r_{2,\max}$, and meanwhile the edge of electrode should be apart from the edge of disk for a certain distance d',

$$R \geqslant r_{2,\max} + d', \tag{9}$$

where the parameters are marked in Fig. 3, and $r_{2,\max}$

is

$$r_{2,\max} = a_2 e^{b\theta_2} = (a_1 + d_{\min}) e^{b\theta_2}. \tag{10}$$

From Eqs. (9) and (10), the limitation of the initial radius of inner edge a_1 is obtained as

$$a_1 \leqslant \frac{(R - d')d_{\min}}{d_{\max}} - d_{\min}, \tag{11}$$

where d' is assumed to be $d_{\min}$, and $R = 38\,\text{mm}$. Equation (11) shows a positive correlation between R and the maximum value of a_1, accordingly the limitation of a_1 is $a_1 \leqslant 14\,\text{mm}$.

Second, the distance between the electrode bars should be not less than the thickness of piezoelectric disk H according to the restrict of fabrication technique

$$r_1' - r_2 \geqslant H, \tag{12}$$

where r_1' and r_2 are marked in Fig. 3, and the expression of r_1' is

$$r_1' = a_1 e^{b(\theta + 2\pi/\ell)}, \tag{13}$$

where ℓ is the topological charger; i.e., the number of electrodes. The thickness of piezoelectric disk H should be not more than half of the wavelength,

$$H \leqslant \lambda_{\min}/2. \tag{14}$$

Assume that H is set to be its maximum value $\lambda_{\min}/2$, i.e., $d_{\min}$, derived from Eqs. (2) and (14). From Eqs. (1), (8), (12) and (13), we can obtain

$$\ell \leqslant \frac{2\pi}{\theta_2} \frac{\ln(d_{\max}/d_{\min})}{\ln(2d_{\min}/a_1 + 1)}, \tag{15}$$

which shows a positive relationship between $\ell_{\max}$ and a_1.

Based on the two geometrical constraint conditions, the limitation of topological charger is derived from Eq. (11) and (15),

$$\ell \leqslant \frac{2\pi}{\theta_2} \ln\left(\frac{d_{\max}}{d_{\min}}\right)\left(\ln\left(\frac{2d_{\max}}{R - d_{\min} - d_{\max}} + 1\right)\right)^{-1}, \tag{16}$$

which indicates that the max topological charger $\ell_{\max}$ increases with the growth of the radius of piezoelectric disk R. In this study, we have $\ell_{\max} = 6$ (Fig. 3) according to the disk radius and frequency bandwidth. It is expected that the largest topological charger is obtained by increasing the radius of piezoelectric disk.

Figures 4 and 5 show the simulation results of the radiated acoustic pressure fields excited by the transducers in Fig. 2, where the observation plane is located at 2.5 wavelengths perpendicular to the piezoelectric transducers in water. Figure 4 is the normalized amplitude distributions of the acoustic pressure for transducers with single-arm to four-arm electrodes, and Fig. 5 is the phase distribution. It can be seen that the structures in Fig. 2 successfully produces acoustic vortices on the observation plane, focusing on the acoustic axis with the topological charge $\ell = 1$, 2, 3 and 4. In the ring of diffraction phase field generated by the transducers with single-arm electrode to four-arm electrode, the phase has changed by 2π, 4π, 6π and 8π, respectively, which proves the topological structure of the corresponding acoustic vortex field.

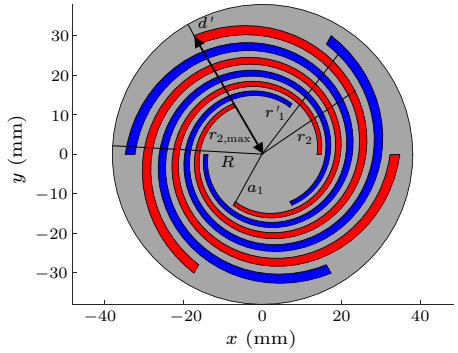

Fig. 3. Simulation models of transducers coated with six-arm coiled spiral electrodes (most electrodes).

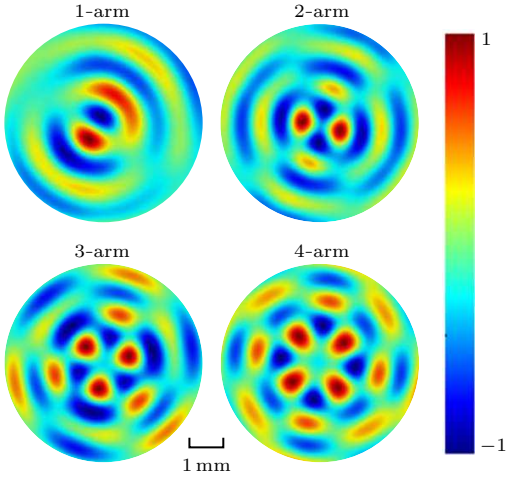

Fig. 4. Normalized amplitude distributions of simulated acoustic pressure field.

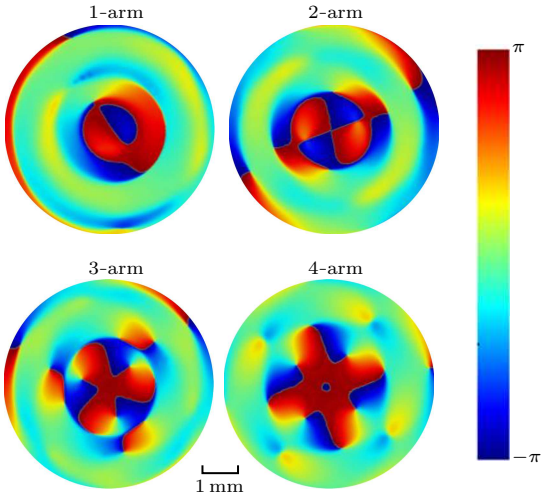

Fig. 5. Phase distributions of simulated acoustic pressure field.

In summary, a method to generate focused acoustic vortex has been proposed based on a piezoelectric

transducer coated with multi-arm coiled electrodes. Finite element simulation results for single-arm to four-arm systems show that the method successfully modulates the amplitude and phase spatial distribution of acoustic wave near the acoustic axis, by the principle of acoustic field synthesis, making the acoustic wave rotate spirally in space and form a stable focused vortex beam. This method has the advantages of compact size, simple operation and generally applicable, breaking through the scale limitation of the traditional active generation of vortex beams with arrays of transducers, and making it possible to miniaturize the active mode. It can be utilized in manipulation and capture of micro-particles, acoustic detection, imaging, and so on. This method has particularly good prospects in medicine.

References

[1] Jiang X, Li Y, Liang B et al 2016 *Phys. Rev. Lett.* **117** 034301
[2] Hong Z Y, Zhang J and Drinkwater B W 2015 *Phys. Rev. Lett.* **114** 214301
[3] Wunenburger R, Lozano J I V and Brasselet E 2015 *New J. Phys.* **17** 103022
[4] Shi C, Dubois M, Wang Y et al 2017 *Proc. Natl. Acad. Sci. USA* **114** 7250
[5] Marzo A, Caleap M and Drinkwater B W 2018 *Phys. Rev. Lett.* **120** 044301
[6] Skeldon K D, Wilson C, Edgar M et al 2008 *New J. Phys.* **10** 013018
[7] Yao A M and Padgett M J 2011 *Adv. Opt. Photon.* **3** 161
[8] Baresch D, Thomas J L and Marchiano R 2016 *Phys. Rev. Lett.* **116** 024301
[9] Lekner J 2006 *J. Acoust. Soc. Am.* **120** 3475
[10] Ren Y, Li L, Wang Z et al 2016 *Sci. Rep.* **6** 33306
[11] Anhäuser A, Wunenburger R and Brasselet E 2012 *Phys. Rev. Lett.* **109** 034301
[12] Courtney C R P, Demore C E M, Wu H, Grinenko A et al 2014 *Appl. Phys. Lett.* **104** 154103
[13] Tran S B Q, Marmottant P and Thibault P 2012 *Appl. Phys. Lett.* **101** 114103
[14] Qi M, Liu J, Mao Y et al 2018 *Chin. Phys. B* **27** 14301
[15] Sun W, Liu G, Xia H et al 2018 *Chin. Phys. B* **27** 84301
[16] Wang S and Lin S 2019 *Acta Phys. Sin.* **68** 024303 (in Chinese)
[17] Xu Z, Qian M, Cheng Q and Liu X 2016 *Chin. Phys. Lett.* **33** 114302
[18] Yu S, Ni X, Xu Y, He C et al 2016 *Chin. Phys. Lett.* **33** 044302
[19] Hefner B T and Marston P L 1999 *J. Acoust. Soc. Am.* **106** 3313
[20] Marchiano R and Thomas J L 2005 *Phys. Rev. E* **71** 066616
[21] Padgett M J 2017 *Opt. Express* **25** 11265
[22] Ealo J L, Prieto J C and Seco F 2011 *IEEE Trans. Ultrason. Ferroelectr. Freq. Control* **58** 1651
[23] Gspan S, Meyer A, Bernet S and Ritsch-Marte M 2004 *J. Acoust. Soc. Am.* **115** 1142
[24] Jiang X, Liang B, Cheng J and Qiu C 2018 *Adv. Mater.* **30** 1800257
[25] Jiang X, Zhao J, Liu S et al 2016 *Appl. Phys. Lett.* **108** 203501
[26] Qian Z, Shang D, Sun Q et al 2019 *Acta Phys. Sin.* **68** 024301 (in Chinese)
[27] Tang J, Piao S and Zhang H 2017 *Chin. Phys. B* **26** 114301
[28] Yang D, Zhang R, Shi S 2018 *Acta Phys. Sin.* **67** 244301 (in Chinese)